Supporting Information

Biologically Inspired Organic Light-Emitting Diodes

Jae-Jun Kim[†,⊥], *Jaeho Lee*[‡], *Sung-Pyo Yang*[†], *Ha Gon Kim*[§], *Hee-Seok Kweon*[‖], *Seunghyup Yoo*[‡], *and Ki-Hun Jeong*[*,†]

[†]Department of Bio and Brain Engineering and KAIST Institute for Optical Science and Technology, Korea Advanced Institute of Science and Technology (KAIST), 291 Daehak-ro, Yuseong-gu, Daejeon 305-701, Republic of Korea

[‡]Department of Electrical Engineering, Korea Advanced Institute of Science and Technology (KAIST), 291 Daehak-ro, Yuseong-gu, Daejeon 305-701, Republic of Korea

[§]Muju Agricultural Technology Center, 416 Hanpungnu-ro, Muju-gun, Jeonbuk 568-802, Republic of Korea

[‖]Division of Electron Microscopic Research, Korea Basic Science Institute, 113 Gwahangno, Yuseong-gu, Daejeon 305-806, Republic of Korea

[⊥]Current Address: Department of Electrical and Computer Engineering, University of Wisconsin-Madison, 1415 Engineering Drive, Madison, Wisconsin 53706, United States

[*]E-mail: kjeong@kaist.ac.kr

Materials and Methods:

OLED Fabrication

Glass substrates precoated with 150nm-thick-ITO layers (<10 Ω/sq, Shinan, Korea, 0.7T) were cleaned in sequence using detergent, DI water, acetone, and isopropyl alcohol in an ultrasonic bath. The cleaned substrates were further treated for 5 min with air-plasma (PDC-32G, Harrick Plasma), and poly(3,4-ethylenedioxythiophene) polystyrene sulfonate (PEDOT:PSS, AI4083) were then spin-coated at 2500 rpm for 30 s on top of the plasma-treated ITO and annealed at 100 °C on a hot plate for 10 min. After annealing, all samples were loaded into a thermal evaporator (HS-1100, Digital Optics & Vacuum) for deposition of buffer layers, organic layers, and metal electrodes. Devices had the following configuration: MoO_3 (5 nm) / 4,4′-Bis(N-carbazolyl)-1,1′-biphenyl (CBP) (20 nm) / CBP : B3PYMPM co-host system (20 nm, 1:1) doped with $Ir(ppy)_2acac$ / bis-4,6-(3,5-di-3-pyridylphenyl)-2-methylpyrimidine (B3PYMPM) (50 nm) / LiF (1nm) / Al (100 nm). The ratio of $Ir(ppy)_2acac$ was set at 7wt %. An bis(2-phenylpyridine)iridium(III)-acetylacetonate ($Ir(ppy)_2acac$) emitter has a maximum electroluminescence (EL) peak at 525 nm (2.36 eV) in the co-host system (CBP:B3PYMPM, 1:1) with PEDOT:PSS and MoO_3 as hole injection layers.

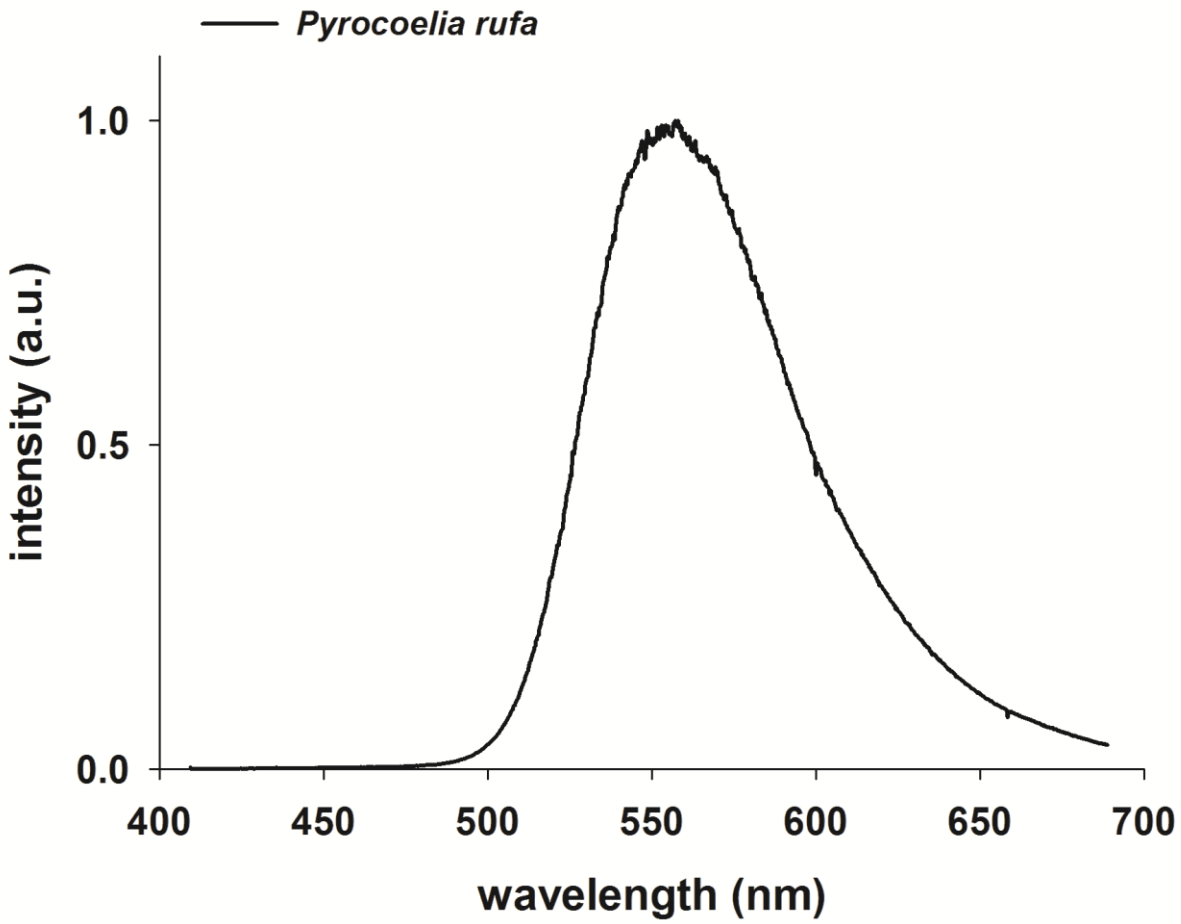

Figure S1. A spectrum of firefly (*Pyrocoelia rufa*) bioluminescence. The spectral peak is around 560 nm in male (72 nm in bandwidth). This spectrum information is used to calculate angular transmittances of a smooth surface, asymmetric microstructures, and hierarchical structures by using a finite difference time domain (FDTD) method.

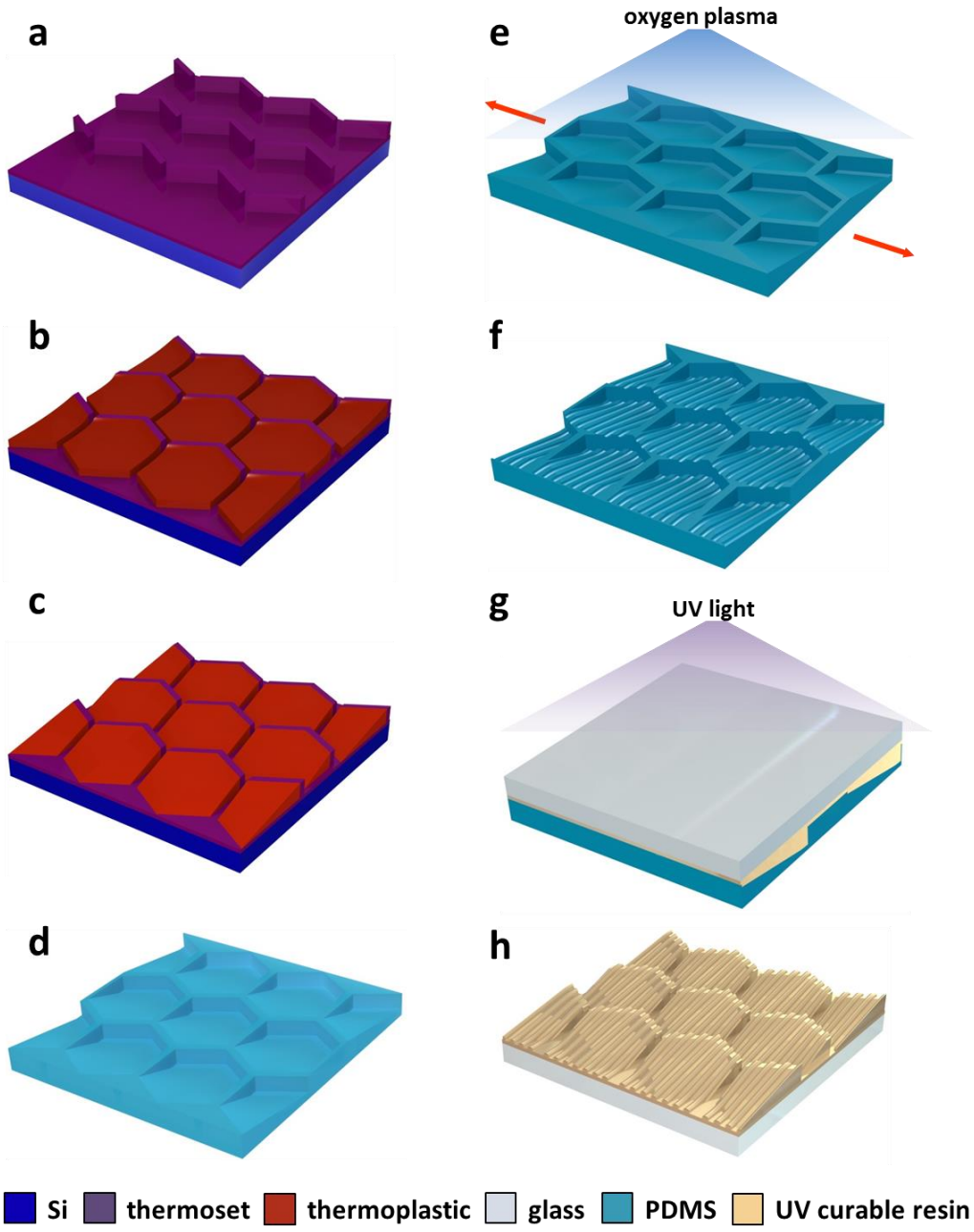

Figure S2. Detailed fabrication procedures of the hierarchical structures. (a) SU-8 patterning. (b) AZ 9260 patterning. (c) Thermal reflow. (d) PDMS replication. (e) Stretching PDMS mold and oxygen plasma treatment. (f) Releasing stretched PDMS. (g) Recasting by UV light curing. (h) Release of hierarchical structures from the PDMS mold.

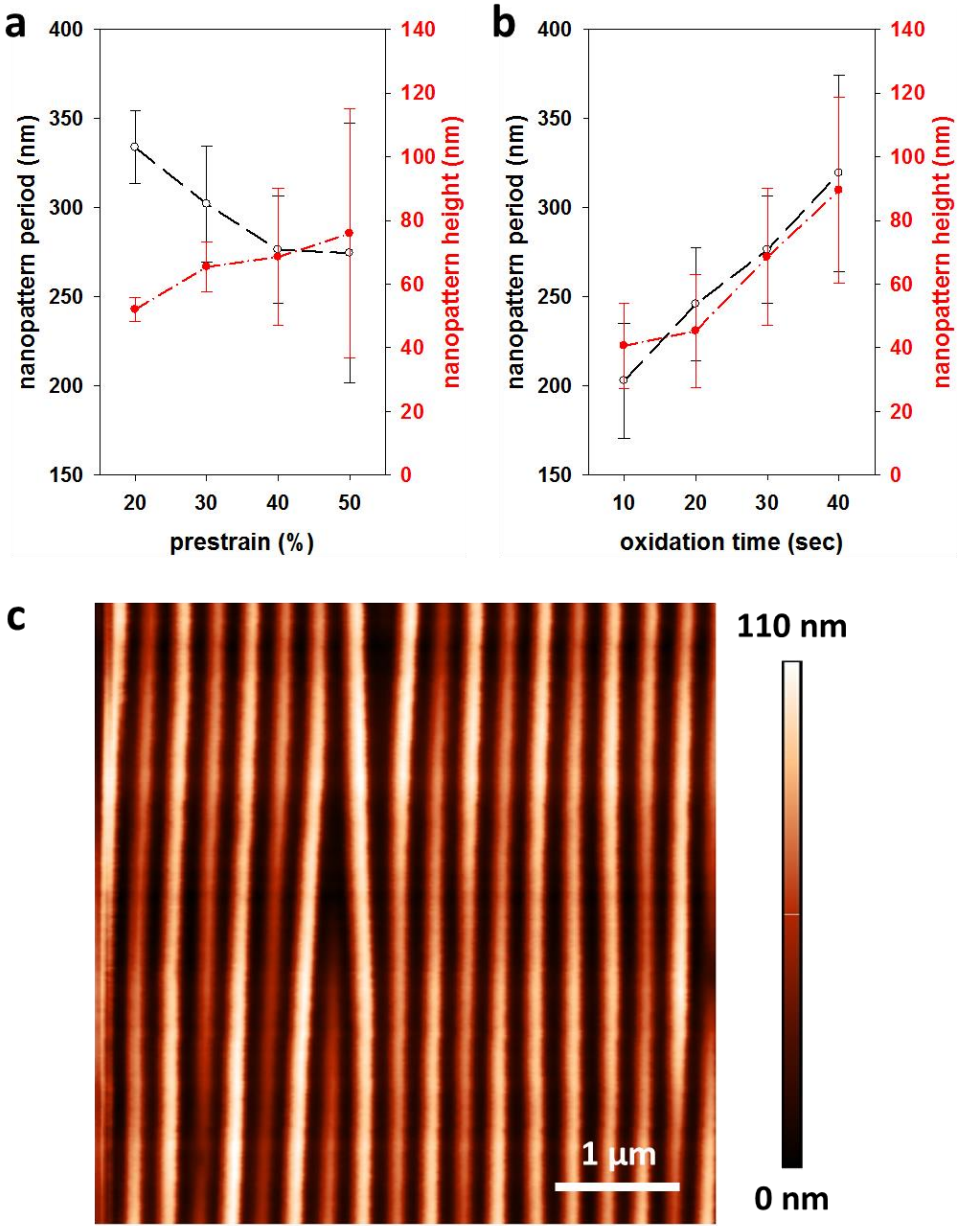

Figure S3. Fabrication conditions of wrinkle nanostructures. The heights and the periods of nanostructures changed by (a) prestrain and (b) oxidation time, respectively. The prestrain and the oxidation time were changed from 20% to 50% and from 10 s to 40 s, respectively. (c) AFM images of a wrinkled nanostructures formed with a pre-stain of 40% and a time of 30 s. The physical dimension of nanostructures is similar to what is founded in a firefly lantern.

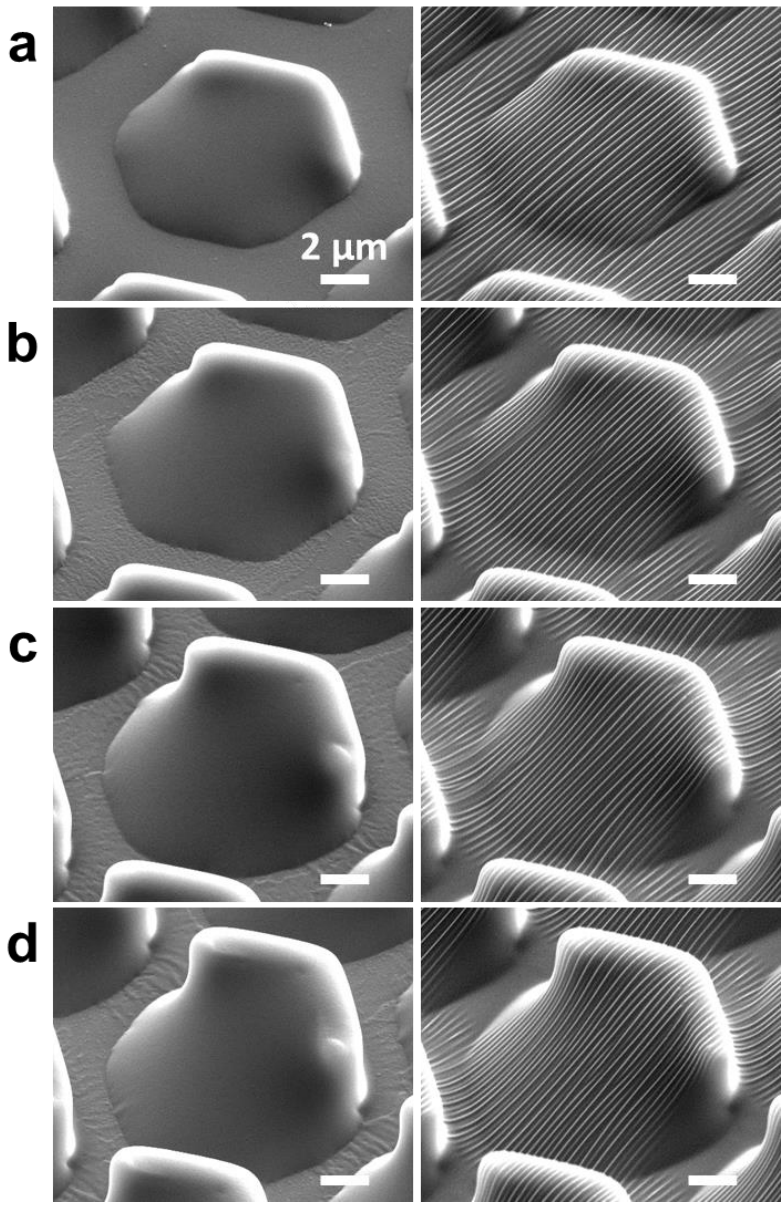

Figure S4. Enlarged perspective SEM images of asymmetric microstructures (left) and hierarchical structures (right) with four different inclined angles. Inclined angles at (a) 5°, (b) 10°, (c) 14°, and (d) 18°. Wrinkle nanostructures were well defined on asymmetric microstructures.

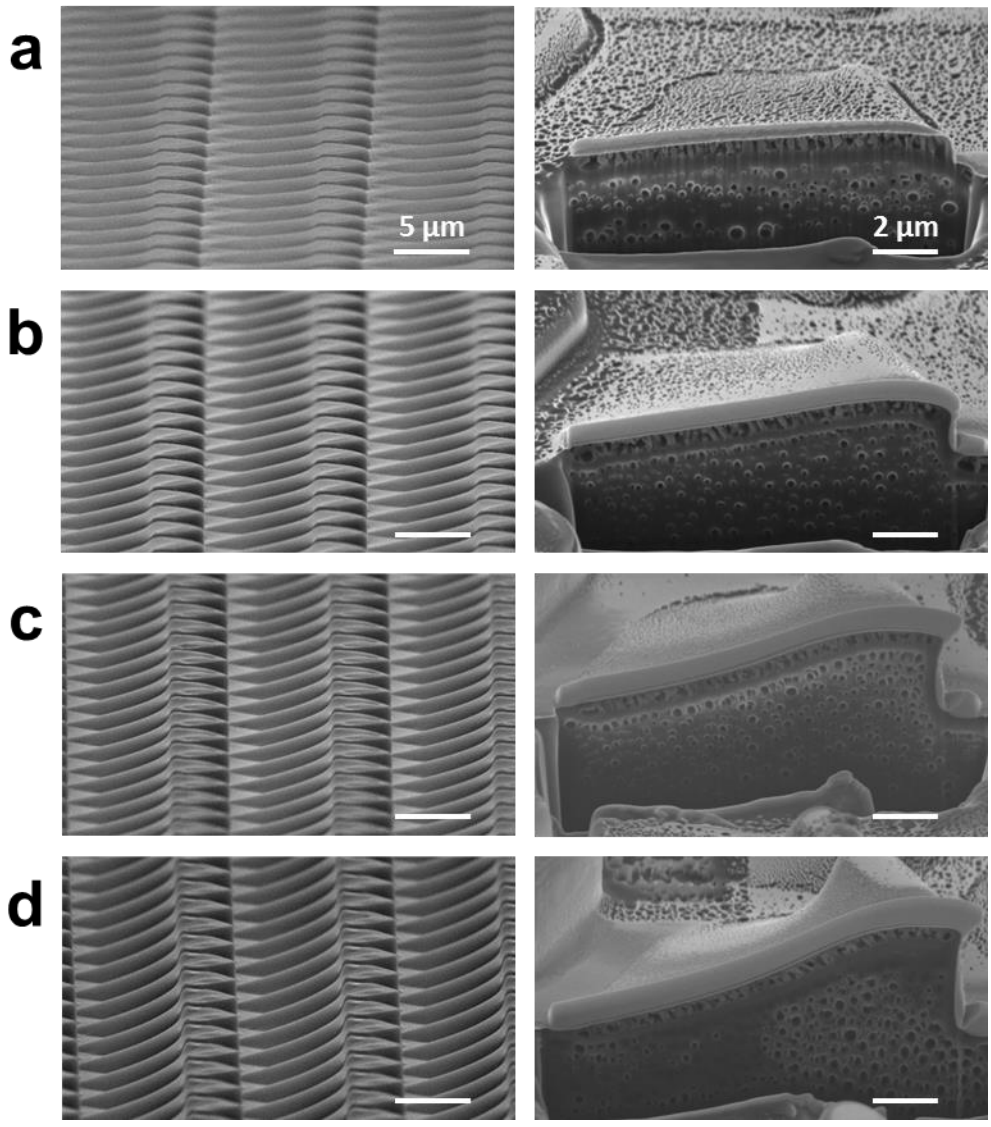

Figure S5. Side-view (left) and the cross-sectional (right) SEM images of asymmetric microstructures with four different heights for (a) 1, (b) 2, (c) 3, and (d) 4 µm under a constant width of 10 µm and a constant gap of 3 µm. The inclined angles are (a) 5°, (b) 10°, (c) 14°, and (d) 18° for different heights of asymmetric microstructures. The cross-sectional SEM images were obtained by using FIB.

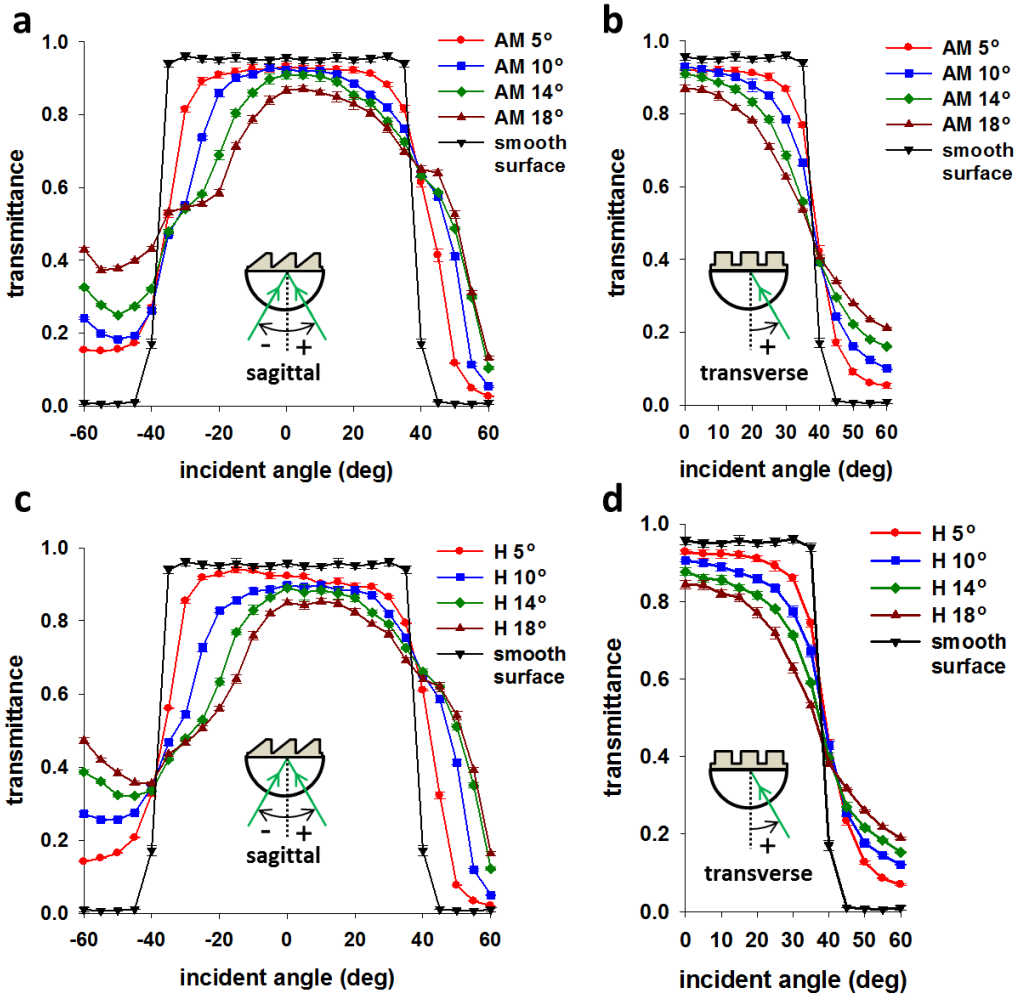

Figure S6. Optical transmittance through asymmetric microstructures and hierarchical structures. Optical transmittance through (a, b) asymmetric microstructures and (c, d) hierarchical structures at different incident angles in the (a ,c) sagittal plane and (b, d) transverse plane. AM, H, and angle values indicate asymmetric microstructures, hierarchical structures, and inclined angles of photonic structures, respectively. Optical transmittance through the structured surfaces is slightly lower than that through the smooth surface for small incident angles but still out-coupled at the incident angles above 40°. In comparison with asymmetric microstructures and hierarchical structures, the transmission increases over the critical angle of TIR but decrease under the critical angle as the inclined angles of microstructures increases.

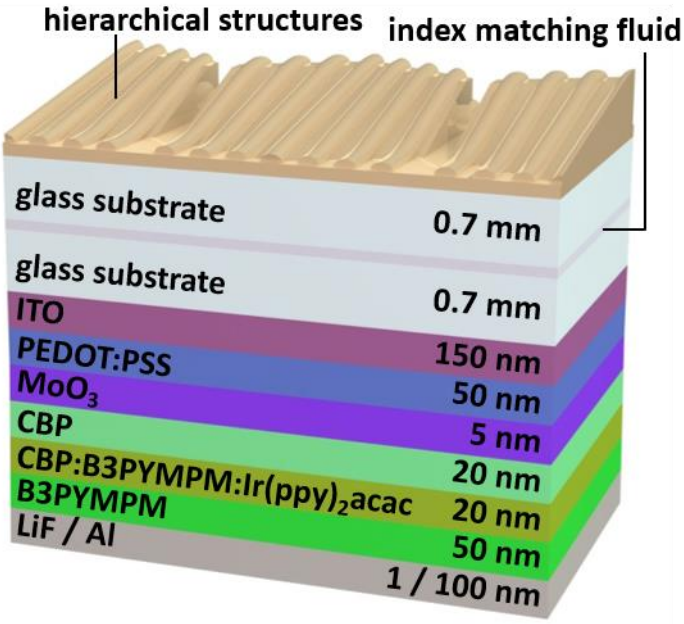

Figure S7. A schematic structure of the OLED with hierarchical structures. The structured surfaces with hierarchical structures were mounted onto the green phosphorescent OLED by adding an index-matching fluid (F-IMF-105, Newport). The OLED devices were based on green phosphorescent emitters of bis(2-phenylpyridine)iridium(III)-acetylacetonate (Ir(ppy)2acac) configured in an exciplex system based on a co-host of CBP and B3PYMPM for energy-efficient performance.

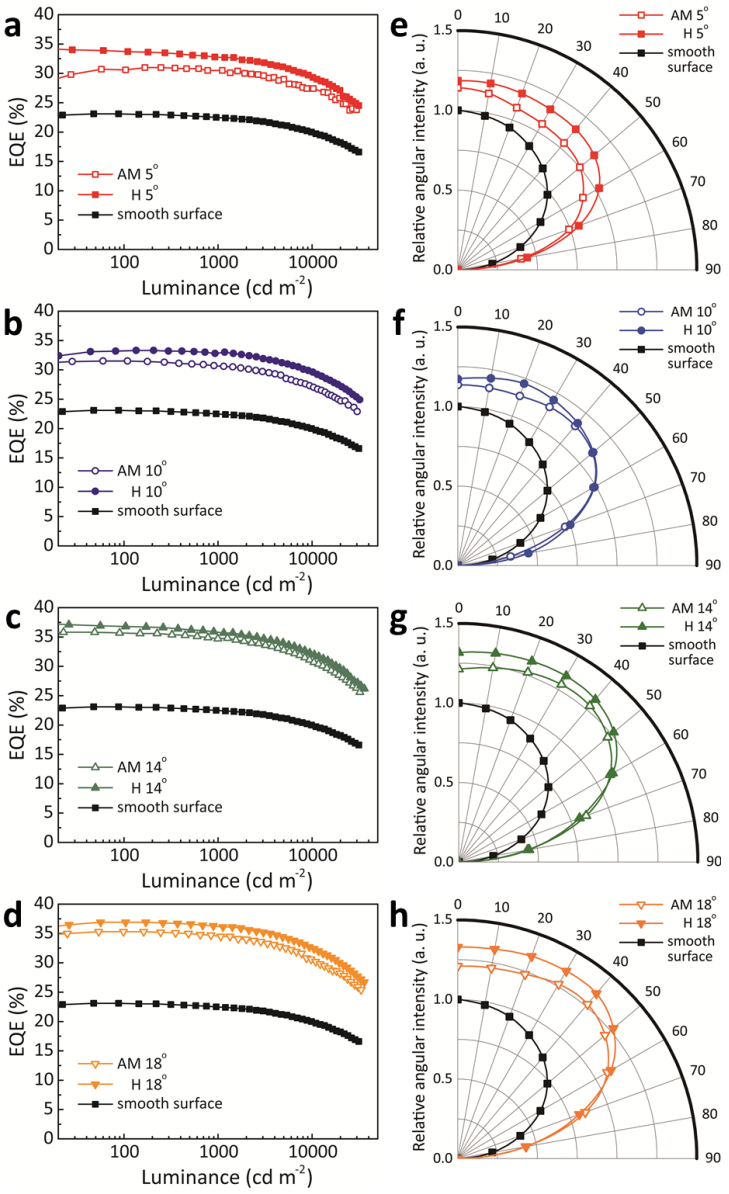

Figure S8. Optical characteristics of an OLED panel with asymmetric microstructures and with hierarchical structures. (a-d) External quantum efficiency (EQE) of an OLED panel versus luminance with smooth surface, asymmetric microstructures, and hierarchical structures at different inclined angles ((a) 5°, (b) 10°, (c) 14°, and (d) 18°). Compared to a smooth surface, hierarchical structures with an inclined angle of 18° exhibit substantially increase of 61% in EQE. Furthermore, the hierarchical structures further improve EQE compared to the asymmetric microstructures at same inclined angles. (e-h) Angular distributions of an OLED panel with

smooth surface, asymmetric microstructures, and hierarchical structures at different inclined angles ((e) 5°, (f) 10°, (g) 14°, and (h) 18°). Both asymmetric microstructures and hierarchical structures clearly show super-Lambertian distribution with side enhancement. The hierarchical structures also show higher angular intensity than asymmetric microstructures at same inclined angles over all angles.

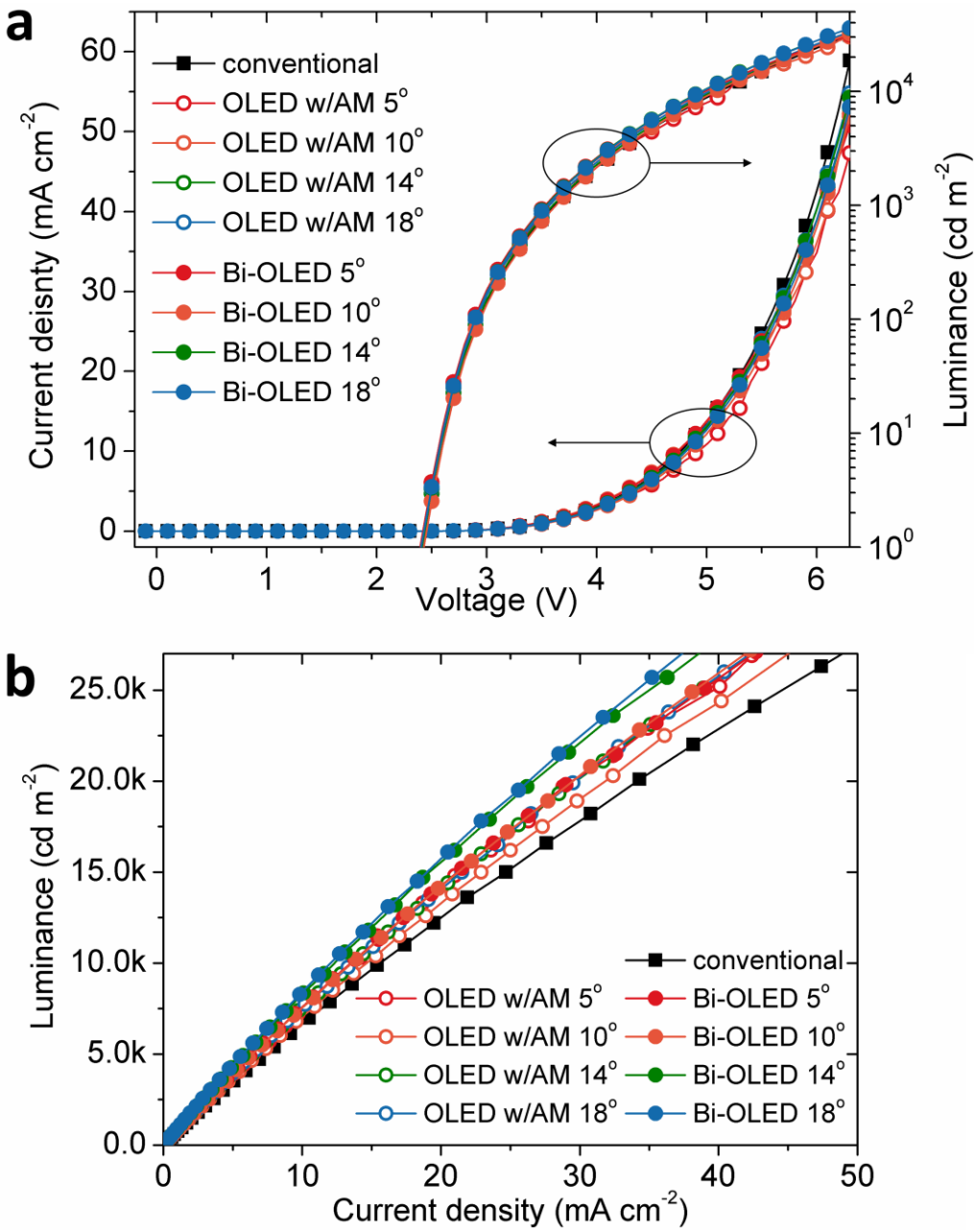

Figure S9. Device performance of the fabricated OLEDs (a) Current density-voltage-luminance (J-V-L) characteristics (b) Luminance-current density (L-J) characteristics. As shown in Fig. S7(a), all devices show similar J-V characteristics whether a photonic structure is used or not. The device with photonic structures shows the enhanced luminance than conventional device at the same current density as shown in Fig. S7(b).

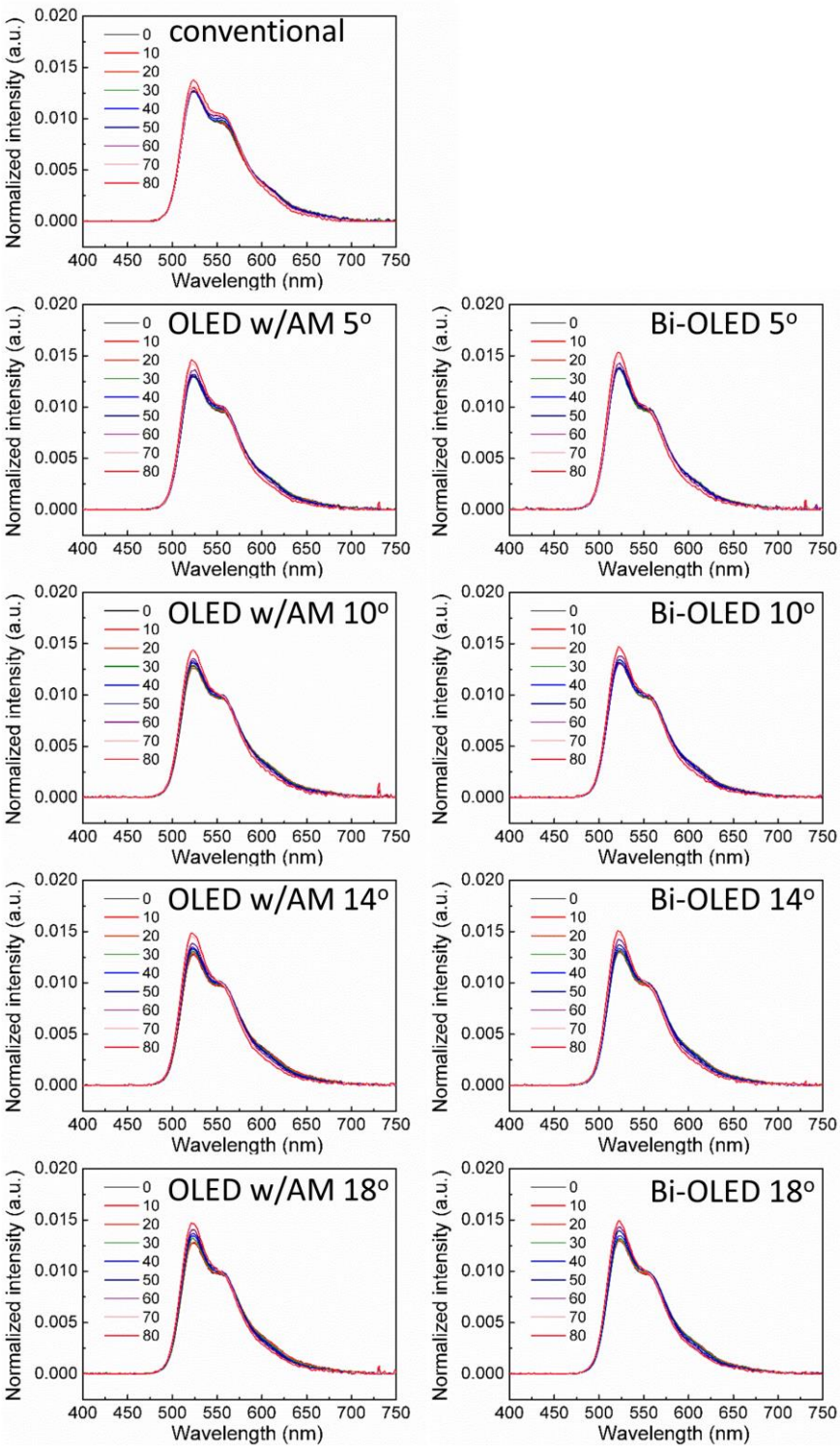

Figure S10. Normalized EL spectra of the OLED devices as a function of viewing angle. All OLED devices show stable angular spectral characteristics.

Table S1. The average transmittances of a smooth surface and structured surfaces. The structured surfaces show lower transmittance than the smooth surface at the incident angles below TIR angle but higher light extraction at the incident angles above TIR angle. The optical transmittance increases at the incident angles above the TIR angle but decreases below the TIR angle as the inclined angle of microstructures increases. The average transmittances of structured surfaces above the TIR angle sufficiently increase compared to a smooth surface. The hierarchical structures can extract more light than asymmetric microstructures due to the subwavelength diffraction of the nanostructures on asymmetric microstructures.

structure	smooth surface	AM 5°	AM 10°	AM 14°	AM 18°	H 5°	H 10°	H 14°	H 18°
total (%)	61	63	62	61	61	63	62	61	59
below TIR angle (%)	90	85	81	76	73	85	80	75	71
above TIR angle (%)	3	17	24	30	36	18	27	32	36

Table S2. The Maximum EQE values (EQE_{max}) of the OLED panels with asymmetric microstructures and with hierarchical structures. The numbers in the parentheses represent the EQE enhancement compared with the EQE of a smooth surface. All Bi-OLEDs show a higher EQE enhancement than OLED w/AM in same inclined angles. The nanostructures formed on the asymmetric microstructures improve light extraction.

type	conventional	OLED w/AM 5°	OLED w/AM 10°	OLED w/AM 14°	OLED w/AM 18°
EQE_{max} (%)	23	31 (35 %)	32 (39 %)	36 (57 %)	35 (52 %)
type		Bi-OLED 5°	Bi-OLED 10°	Bi-OLED 14°	Bi-OLED 18°
EQE_{max} (%)		34 (48 %)	33 (43 %)	37 (61 %)	37 (61 %)